Faraday Discussions

Accepted Manuscript

This manuscript will be presented and discussed at a forthcoming Faraday Discussion meeting. All delegates can contribute to the discussion which will be included in the final volume.

Register now to attend! Full details of all upcoming meetings: http://rsc.li/fd-upcoming-meetings

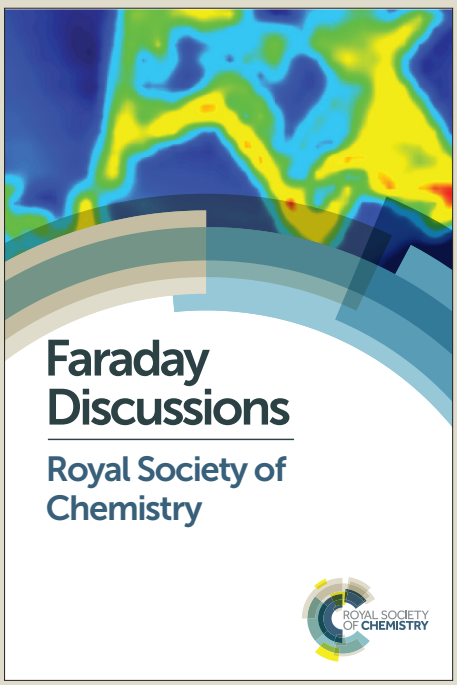

This is an *Accepted Manuscript*, which has been through the Royal Society of Chemistry peer review process and has been accepted for publication.

Accepted Manuscripts are published online shortly after acceptance, before technical editing, formatting and proof reading. Using this free service, authors can make their results available to the community, in citable form, before we publish the edited article. We will replace this *Accepted Manuscript* with the edited and formatted *Advance Article* as soon as it is available.

You can find more information about *Accepted Manuscripts* in the Information for Authors.

Please note that technical editing may introduce minor changes to the text and/or graphics, which may alter content. The journal's standard Terms & Conditions and the Ethical guidelines still apply. In no event shall the Royal Society of Chemistry be held responsible for any errors or omissions in this *Accepted Manuscript* or any consequences arising from the use of any information it contains.

ROYAL SOCIETY OF CHEMISTRY

www.rsc.org/faraday_d

Please do not adjust margins

Faraday Discussions

ARTICLE

Ozone Production Chemistry in the Presence of Urban Plumes

W. H. Brune[a], B. C. Baier[a], J. Thomas[a,b], X. Ren[c], R. C. Cohen[d], S. E. Pusede[d,e], E. Browne[d,f], A.H. Goldstein[g], D. R. Gentner[h], F. N. Keutsch[i], J. Thornton[j], S. Harrold[j,k], F. Lopez-Hilfiker[j,l], P. O. Wennberg[m]

Received 00th January 20xx,
Accepted 00th January 20xx

DOI: 10.1039/x0xx00000x

www.rsc.org/

Ozone pollution affects human health, especially in urban areas on hot sunny days. Its basic photochemistry has been known for decades and yet it is still not possible to correctly predict the high ozone levels that are the greatest threat. The CalNex_SJV study in Bakersfield CA in May/June 2010 provided an opportunity to examine ozone photochemistry in an urban area surrounded by agriculture. The measurement suite included hydroxyl (OH), hydroperoxyl (HO_2), and OH reactivity, which are compared with the output of a photochemical box model. While the agreement is generally within combined uncertainties, measured HO_2 far exceeds modeled HO_2 in NO_x-rich plumes. As a result, OH production and loss do not balance as they should in the morning and the ozone production calculated with measured HO_2 is a decade greater than that calculated with modeled HO_2 when NO levels are high. Calculated ozone production using measured HO_2 is twice that using modeled HO_2, but this difference in calculated ozone production has minimal impact on the assessment of NO_x-sensitivity or VOC-sensitivity for ozone production. Evidence from this study indicates that this important discrepancy is not due to the HO_2 measurement or to the sampling of transported plumes but instead to either emissions of unknown organic species that accompany the NO emissions or unknown photochemistry involving nitrogen oxides and hydrogen oxides, possibly the hypothesized reaction $OH+NO+O_2 \rightarrow HO_2+NO_2$.

Introduction

Ground-level ozone (O_3) is a serious health hazard[1,2], with no known safe limit, and is estimated to cause millions of deaths per year globally. In the United States, urban ozone levels have decreased dramatically in the past two to three decades due to the significant investments made in understanding the cause of ozone pollution and to air quality regulations[3]. These regulations have encouraged lower emissions of nitrogen dioxide (NO_2) and nitric oxide (NO) (collectively termed NO_x) and volatile organic compounds (VOCs), which are the raw ingredients needed to produce ozone. Although ozone reductions in some parts of the United States appear to have leveled off, ozone reduction in the United States is a success story-one that should be emulated globally. However, with limited resources, much of the world cannot afford the investment the United States has made. The solution is an optimized approach that can target the specific emissions to which ozone production is most sensitive.

An optimized approach to ozone pollution reduction requires a solid scientific understanding of the causes of ozone pollution. The basic chemistry has been known for decades.[4,5,6] Ozone production begins with the early morning production of the hydroxyl (OH) and hydroperoxy (HO_2) radicals in the presence of NO_x (NO_2 + NO) and VOC emissions. Hydroxyl reacts with the VOCs, causing a cascade of reactive organic compounds, including organic peroxy radicals (RO_2) and HO_2. The peroxy radicals react with NO to form peroxy radicals and NO_2. Nitrogen dioxide is decomposed by ultraviolet sunlight to form NO and atomic oxygen, which immediately reacts with molecular oxygen (O_2) to form ozone. This process is the dominant production pathway for tropospheric ozone.

[a] Department of Meteorology, Pennsylvania State University, University Park, PA 16802.
[b] Department of Earth and Planetary Sciences, Johns Hopkins University, Baltimore, MD 21218.
[c] NOAA Air Resources Laboratory, College Park, MD, 20740.
[d] Departments of Chemistry and Earth and Planetary Science, University of California, Berkeley, CA 94720.
[e] Department of Environmental Sciences, University of Virginia, Charlottesville, VA 22904.
[f] Department of Chemistry and Biochemistry, University of Colorado, Boulder, CO 80309
[g] College of Natural Resources, University of California, Berkeley, CA 94720.
[h] Department of Chemical and Environmental Engineering, Yale University, New Haven, CT 06511
[i] Department of Chemistry and Chemical Biology, Harvard University, Cambridge, MA 02138.
[j] Department of Atmospheric Sciences, University of Washington, Seattle, WA 98195.
[k] Puget Sound Clean Air Agency, Seattle, WA 98101.
[l] Paul Scherrer Institut, Villigen PSI, Switzerland.
[m] Division of Geological and Planetary Sciences, Caltech, Pasadena, CA 91125.
† Footnotes relating to the title and/or authors should appear here.
Electronic Supplementary Information (ESI) available: [details of any supplementary information available should be included here]. See DOI: 10.1039/x0xx00000x

Faraday Discussions Accepted Manuscript

Please do not adjust margins

However, NO also reacts with O_3 to make NO_2, NO and NO_2 come into a steady-state balance within tens of seconds, and NO_2 then reacts with OH to terminate NO_x and HO_x (OH + HO_2) cycling. By this theory, the instantaneous ozone production, $P(O_3)$, initially increases as NO increases, but then decreases with continued NO increase. The peak $P(O_3)$ is a sensitive function of HO_x production.[7,8,9] One simple test of the non-linear dependence of ozone production on NO_x is the so-called weekend-weekday effect, for which ozone is greatest on weekends when NO_x is less.[10]

Despite this well-accepted theory, there are discrepancies between measured and ozone calculated by regional air quality models. The models agree with the observations on average, but tend to be too high for values below 50 ppbv and too low for values approaching 80-90 ppbv and beyond. While models have had better agreement with observations for individual cities and times of the year, this discrepancy between modeled and measured ozone is found for several different models and urban areas.[11,12,13] The causes of the disagreements between measured and modeled ozone are usually attributed to errors in the emissions inventories for nitrogen oxides (NO_x) and volatile organic compounds (VOCs), but there is some evidence that the well-tested theory may need some modification.

The budget equation for ozone is

$$\frac{\partial[O_3]}{\partial t} = P_{chem} - L_{chem} + \frac{w_e \Delta O_3 - u_d[O_3]}{H} - \nabla \cdot (\boldsymbol{v}[O_3]), \qquad (1.1)$$

where P_{chem} is the chemical O_3 production rate, L_{chem} is the loss rate, $w_e \Delta O_3$ is the ozone entrainment rate between the mixing layer and the free troposphere, $u_d[O_3]$ is the ozone deposition rate, H is the mixing layer height, and $\nabla \cdot (\boldsymbol{v}[O_3])$ is the ozone advection rate by the mean wind, $\boldsymbol{v}$. Net ozone production can be calculated from 1.2-1.4,

$$P(O_3) = P_{chem} - L_{chem} \qquad (1.2)$$

$$P_{chem} = k_{NO+HO_2}[NO][HO_2] + \sum_i k_{NO+RO_{2i}}[NO][RO_{2i}] \qquad (1.3)$$

$$L_{chem} = f_{H_2O} J_{O_3}[O_3] + k_{O_3+OH}[O_3][OH] + k_{O_3+HO_2}[O_3][HO_2] + k_{NO_2+OH}[NO_2][OH] + L(O_3 + alkenes) + L(O_3 + halogens) + P(RONO_2) \qquad (1.4)$$

where *k's* are rate coefficients; *NO* is nitric oxide; HO_2 is the hydroperoxyl radical; RO_2 is organic peroxyl radical; J_{O3} is the photolysis frequency of O_3; f_{H2O} is the fraction of the excited state $O(^1D)$ atoms from O_3 photolysis that react with H_2O; *OH* is the hydroxyl radical; and $RONO_2$ represents organic nitrates.

In several studies, the measured HO_2 often is less than modeled HO_2 at low NO, equals modeled HO_2 when NO was about 1 ppbv, and increasingly exceeds modeled HO_2 at increasingly higher NO abundances.[14,9,15,16,17,18] This measured-to-modeled difference is greatest when HO_x production is lowest, such as during morning rush hour, where the measured-to-modeled HO_2 ratio can be higher than ten. It is least when HO_x production is greatest, such as during the afternoon. This greater-than-expected HO_2 at higher NO is also inferred from peroxynitric acid (HO_2NO_2) measurements in Mexico City in 2006.[19] Therefore, ozone production (PO_3) calculated using the measured HO_2 can exceed $P(O_3)$ calculated using the modeled HO_2. In addition, a direct measurement of the ozone production rate shows that measured $P(O_3)$ is twice $P(O_3)$ calculated using modeled HO_2 and RO_2, although the timing of the $P(O_3)$ peak agrees better with the $P(O_3)$ calculated with modeled HO_2 than with $P(O_3)$ calculated with measured HO_2.[20,21] These observations are inconsistent with the current understanding of ozone production.

This discrepancy can be explained in several different ways. A first hypothesis is that the HO_2 measurement is being affected by the atmospheric NO levels. A second hypothesis is that calculation of $P(O_3)$ is being distorted by the averaging over plumes of NO_x-rich and HO_2-rich air so that the product of averaged measured $[HO_2]$ and [NO] is larger than the average of the products of the plume-scale NO and HO_2:

$$\overline{[HO_2]}\,\overline{[NO]} > \overline{[HO_2][NO]}\,. \qquad (1.5)$$

A third hypothesis is that HO_x measurements made when NO_x is not in photostationary state (PSS) are being compared to models that calculate HO_x while assuming NO_x photostationary state. Because NO_x is typically emitted from combustion as NO, the HO_x loss due to OH+NO_2 would be less than in the model and measured HO_2 would appear to be greater than modeled. The fourth hypothesis suggests that unknown HO_x sources are co-emitted with the NO_x. The fifth hypothesis is that unknown chemistry is missing from the current understanding of the chemistry between nitrogen oxides and hydrogen oxides.

The multi-agency California Research at the Nexus of Air Quality and Climate Change- San Joaquin Valley (CalNex-SJV) study in Bakersfield CA during June 2010 meets the criteria needed to test these hypotheses. Bakersfield is situated in the southern San Joaquin Valley 180 km north-northwest of Los Angeles and experiences the second worst ozone pollution in California.[22] It is surrounded by agricultural land, but at the same time has active oil/gas fields and an oil refinery and significant traffic on highways that has a higher fraction of diesel powered vehicles than other urban areas in the U.S.[23] Its numerous point and distributed NO_x and VOC emission sources create a heterogeneous mix of plumes of different sizes and chemical composition. This combination of high VOC and NO_x emissions and the typically cloudless, hot weather causes high ozone abundances. Bakersfield CA typically has 90 exceedances of ozone air quality standards each year and, while the number has decreased during the past decade, it is still not in compliance with EPA air quality standards.[22]

The calculated ozone production has been examined for the San Joaquin Valley (SJV), including Bakersfield. In a study using midday measurements of temperature as a surrogate for OH reactivity from VOCs, NO_x, and frequency of O_3 exceedances, Pusede and Cohen showed that the calculated $P(O_3)$ is consistent with a transition from VOC-sensitive to NO_x-sensitive regimes for much of the SJV,

Faraday Discussions Accepted Manuscript

 This journal is © The Royal Society of Chemistry 2015

starting first with higher maximum daytime temperatures (34-45°C) followed by the beginning of a transition at more moderate temperatures (28-33°C).[24] In a second study focused on the CalNex-SJV site, Pusede et al.[25] show that $P(O_3)$ calculated with an analog model is NO_x-sensitive for moderate-to-high temperatures, except weekdays at moderate temperatures, for which it is VOC-sensitive. These conclusions appear to be inconsistent with the $P(O_3)$ calculated from the measurements of HO_2 and RO_2 as a function of NO described above. However, high NO and greater-than-expected $P(O_3)$ occur mainly in the morning before 10:00 and it is not clear how this difference will affect the averaged $P(O_3)$ sensitivity to NO_x and VOCs calculated for midday.

In this paper, we will test these hypotheses using primarily the HO_2 and NO abundances measured during CalNex-SJV. First we will compare the measured OH, HO_2, and OH reactivity to those calculated by a near-explicit box model that is constrained by all other simultaneous field measurements in Bakersfield. Measured and modeled OH production and loss rates and ozone production from HO_2 are also compared and discussed. Finally we add the evidence learned from this study to that from previous studies to assess the likelihood of the hypotheses for the greater-than-expected ozone production at greater NO abundances.

Methods

Measurement Site

The CalNex 2010 field campaign in California consisted of aircraft and ship measurements, as well as two ground sites: one in Pasadena CA and a second in Bakersfield CA. This work focuses on the CalNex-SJV Bakersfield site. A scaffolding tower 18 m high was erected in a field just to the east of a parking lot at the California Agricultural Experiment Station, which is located in south Bakersfield (35.346153 N, 118.965519 W). The land to the south is fields and settling ponds. Light businesses were located to the north, along with highway 58, a highly trafficked corridor, about 760 m away. A school bus facility was also located 600m to the west.

Measurements were made from 15 May to 28 June 2010. For that time of year, the weather in Bakersfield is typically hot and dry, with temperatures routinely exceeding 37°C. However, 2010 was not a typical year. The temperature did not exceed 35°C until the last three days, and during one week, the weather was cloudy with some light rain with temperatures ranging from 20°C and to 25°C. Winds were generally from the north at 4 ms^{-1}, although they were often calm and from the east in the hours around sunrise.

HO_x Measurements

OH and HO_2 were measured with Penn State's Ground-based Tropospheric Hydrogen-Oxides Sensor (GTHOS),[26] which uses laser-induced fluorescence (LIF). The hydroxyl radical (OH) is detected as the sampled air is pulled through a 1-mm inlet into low pressure (~6 hPa) and passes through the path of a laser tuned to the $Q_1(2)$ OH absorption line at 308 nm, and then fluoresces. This fluorescence is measured in a first detection axis by a gated microchannel plate detector positioned perpendicular to the sample flow and the laser beam. The sampled air flows out of the first detection axis, has NO injected into it to react with HO_2 to form OH, which is then detected by LIF in a second detection axis in order to detect HO_2.

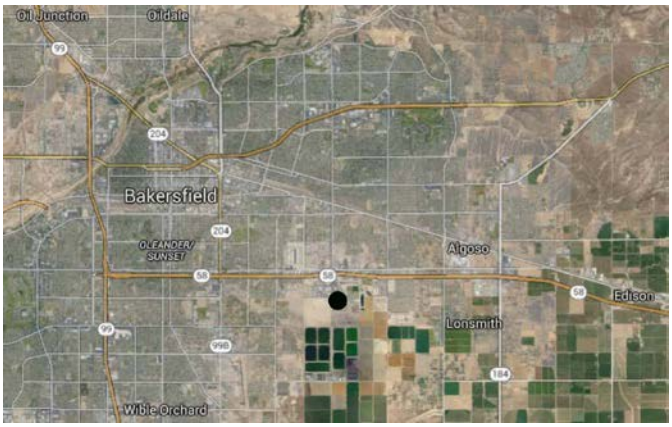

Figure 1. Map of Bakersfield CA and location of the CalNex-SJV site (black dot) (Google, 2015). The site was at 35.346153°N and 118.965519°W. The heavily traveled four-lane highway 58 was located 760 m to the north of the site. The nearest local road, East Belle Terrace, was 50 m to the north and had light traffic during the study period.

A tunable dye laser pumped by a 532 nm Nd:YAG laser produces the 308 nm light used to detect OH. This laser wavelength is alternately tuned by an etalon to a wavelength were OH absorbs and then fluoresces or to the background on alternate sides of the OH absorption line, all within a 30-second cycle. The difference between these two signals is proportional to OH. The proportionality constant is determined by laboratory and field calibrations.[26] This method of measuring OH is referred to as OH_{wave}. Wavelength modulation has been the most common method for measuring atmospheric OH by LIF.

A second OH measurement method involves injecting an OH reactant into the air to scavenge the OH before it is sampled through the instrument inlet. Reactant amounts are chosen to maximize the fraction of OH removed in the 10 ms between injection and entering the inlet and to simultaneously minimize the OH removed inside the instrument. Hexafluoropropylene (C_3F_6) was used as the OH scavenger. By turning C_3F_6 injection on and off, the OH signal is found by subtracting the signal when injection is on from the signal when injection is off. This method is called OH_{chem}. The difference between OH_{wave} and OH_{chem} is the OH from an interference, called OH_{int}. The OH interference has the spectral signature of OH, but all studies show that it is not laser-generated. To test the functionality of the OH_{chem} system, a UV lamp was affixed to the instrument near the inlet. The lamp, which photolyzed water vapor to make a large OH signal, was turned on for a few minutes three times a day to ensure that the C_3F_6 injection was scavenging OH properly. For this paper, the OH measurements were all made with the chemical removal method.

Two years after CalNex-SJV, it was reported that some alkene-based and aromatic-based organic peroxides were also detected along with HO_2 in most instruments that used NO to convert HO_2 to OH.[27] Methods have been found to minimize this interference, but these methods were not used in the CalNex-SJV study. This sum of HO_2 and a subset of RO_2 has been called HO_2^*, which is then compared to modeled HO_2^*.[28] In this paper, our approach is to bound the possible HO_2 values by subtracting all the modeled RO_2 from HO_2^* and calling this value HO_2, which may be an overcorrection. This

Faraday Discussions Accepted Manuscript

HO_2 is actually the lower bound of HO_2 and HO_2* is the upper bound. As will be seen, the main conclusions are not sensitive to the choice of HO_2 between these two bounds.

In addition to OH and HO_2 measurements, measurements were also made of OH reactivity, which is the inverse of the OH lifetime.[29,30] Approximately 150 LPM of ambient air is drawn into the instrument and flows through the aluminum flow tube (7.5 cm dia.). At the far end of the flow tube is a sampling inlet and an OH measurement system nearly identical to the one used in the main GTHOS system. Before the airflow reaches the sampling inlet, it flows past a movable source of OH called the wand. Inside the wand, 5 LPM of moist nitrogen flows past a mercury lamp, which photolyzes the water vapor to produce OH and HO_2 and then jets out detection axis. As the wand is moved farther away from the sampling inlet, the OH has more time to react with trace gases in the ambient air flowing through the tube and the OH signal decreases exponentially. Moving 10 cm is equivalent to a decay time of 140 ms and the wand completes a cycle in 30 seconds. The OH reactivity is the slope of the change in the log of the OH signal divided by the reaction time.

The OH reactivity decay is affected by atmospheric NO because HO_2+NO→OH+NO_2 recycles OH that has decayed, thus causing curvature in the OH decay. A least-squares linear fit to this curved decay produces a decay slope that is less than the real slope and thus produces an OH reactivity value that is too low. The effects of atmospheric NO on the OH reactivity measurement is minimized by applying the correction algorithm described in Shirley et al.[31]

A suite of measurements at the CalNex-SJV site was extensive as documented in the CalNex overview paper.[32] It included meteorological parameters, inorganic species, volatile organic compounds (VOCs) and oxygenated VOCs, and many aerosol abundances and properties. Data used in this study were drawn primarily from measurements taken at or near the top of the measurement tower.

Photochemical Box Modeling

The simultaneous measurements of all available inorganic and organic species and meteorological parameters were used to calculate HO_x using the near-explicit Master Chemical Mechanism, Version 3.2 (MCMv3.2)[33] in a box model framework developed by G. Wolfe[34]. MCMv3.2 contains approximately 6,700 unique chemical species and 17,000 reactions. Measured VOCs that are included in the model are treated explicitly; those that are not represented in the model are aggregated into appropriate MCMv3.2 species based on OH-reactivity or their molecular structure. It should be noted that isoprene chemistry in MCMv3.2 is replaced with explicit reactions detailed in Mao et al.[35]. Chemical species were assumed to have a lifetime of one day to prevent buildup in the model. Data were then averaged into ten-minute time intervals for the modeling and the comparisons to measurements.

Photolysis frequencies were not measured during CalNex-SJV, so instead they were calculated using the NCAR Tropospheric Ultraviolet and Visible Radiation Model[36]. These calculations assume clear overhead skies with overhead the overhead ozone column of 300 D.U. taken from satellite measurements; to correct for the effects of overhead cloud cover, photolysis frequencies were scaled by the ratio of the calculated JNO_2 to JNO_2 measured from a UV radiometer on the measurement tower. This same cloud correction factor was applied to the other calculated photolysis frequencies and has been shown to give accurate photolysis frequencies.[37]

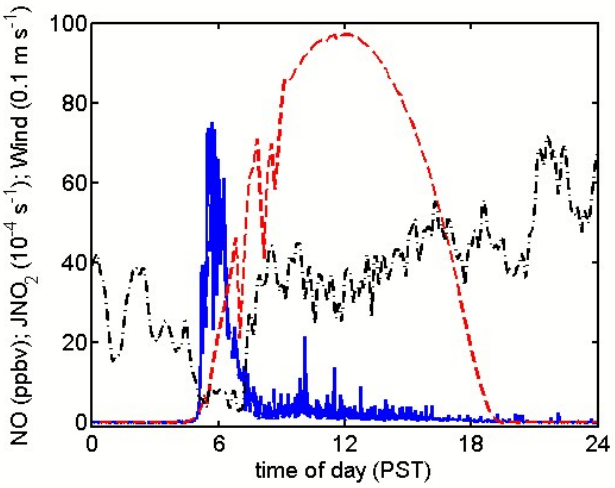

Figure 2. Behavior of measured NO (blue solid line), J(NO_2) (red dashed line), and wind speed (dot-dashed black line) for day-of-the-year (doy) 160, 9 June. This behavior is typical for most days during the study period, although NO bump on doy 160 was one of the largest. The width of the NO spikes range from seconds to hours.

Model results include days between 23 May and 28 June 2010 to allow for the greatest number of simultaneously measured chemical species to constrain the model. Data were taken from three periods when HO_x, OH reactivity, and other chemical species important for this analysis were being measured: doy 145-150; doy 156-164; and doy 166-174. They were averaged or interpolated into 10-minute time intervals for the model runs. For analysis of HO_x and $P(O_3)$ as a function of NO, the 10-minute data were limited to hours between 7:00 and 17:00, a time period chosen to capture the portion of morning rush hour in which the photolysis and transport were well defined. All times are Pacific Standard Time even though the official time was Pacific Daylight Time during the field study.

CalNex-SJV measurement and model uncertainties

The absolute uncertainties for OH and HO_2 are approximately ±40% at the 2σ confidence level. However, the subtraction of the OH signals with and without C_3F_6 scavenging causes the OH limit-of-detection to be about (2-3)x10^5 cm^{-3}. In addition, with the RO_2 interference in the HO_2 measurement, there is an additional uncertainty that can be about a factor of two. In studies after CalNex, our measurement strategy was revised to minimize the RO_2 interference in the HO_2 measurement. The uncertainty for the OH reactivity instrument is estimated to be ±30% at 2σ confidence. The uncertainties in the other measurements are given in Table 7a of the overview paper[32]. The model uncertainty can be estimated from a global uncertainty and sensitivity analysis from a previous urban study using the RACM2 model.[38] These two studies have similar uncertainties in their input measurements, reaction rate coefficients, and products, so the uncertainties in the modeled OH and HO_2 for comparable urban areas should also be similar. Thus,

Faraday Discussions Accepted Manuscript

 This journal is © The Royal Society of Chemistry 2015

the estimated 2σ uncertainty is approximately 40% for OH and HO_2. These uncertainties will be used to assess the significance of the comparisons between the measured and modeled OH, HO_2, and OH reactivity in this study.

Results

Comparison of Measured and Modeled OH and HO_2

Understanding ozone production requires an understanding of OH and HO_2. A first-order test of this chemistry is the comparison of the modeled and measured OH and HO_2 as a function of the time of day (Figure 3).

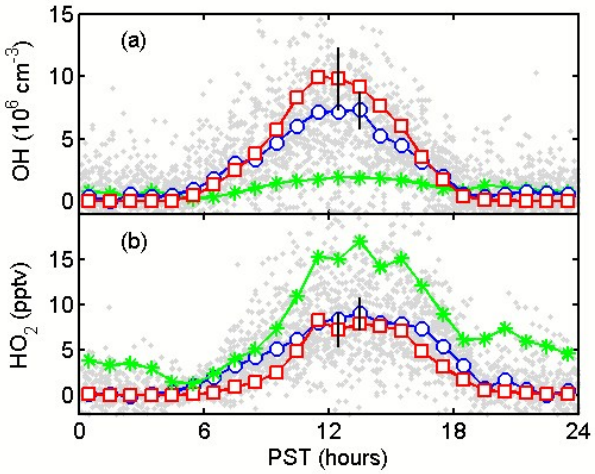

Figure 3. Median diel variation of HO_x. (a) OH (10^6 cm^{-3}), measured (blue circles), modeled (red squares), and OH interference (green stars), with individual 10-min data for measured OH (gray dots); (b) HO_2 (pptv), measured (blue circles), modeled (red squares), and measured HO_2 with the RO_2 interference (green stars), with individual 10-min data for measured HO_2 (gray dots). Error bars are ±1σ confidence.

The median measured and modeled OH display the same diel behavior but the measured OH peaked at (7.3±2.5)x10^6 cm^{-3} while the modeled OH peaked at (10.4±4.0)x10^6 cm^{-3}. This marginal statistical difference of ~30% persists during the midday, although at sunrise and sunset, the modeled and measured OH agree. At night, the median measured OH is 3x10^5 cm^{-3}, which is near the instrument detection limit and is consistent with the modeled nighttime OH of 3x10^4 cm^{-3}.

The OH interference signal peaks midday at 2x10^6 cm^{-3}, is about 1x10^6 cm^{-3} at night, and is only about 25% of the OH determined by the chemical removal method. Interestingly, this OH interference signal is about the same as that observed in forests[35,39] and in other cities[17] and may have a common origin, but because the OH is about 10 times larger in cities than in forests, the interference's effect of the measured OH is much more significant in forests than in cities.

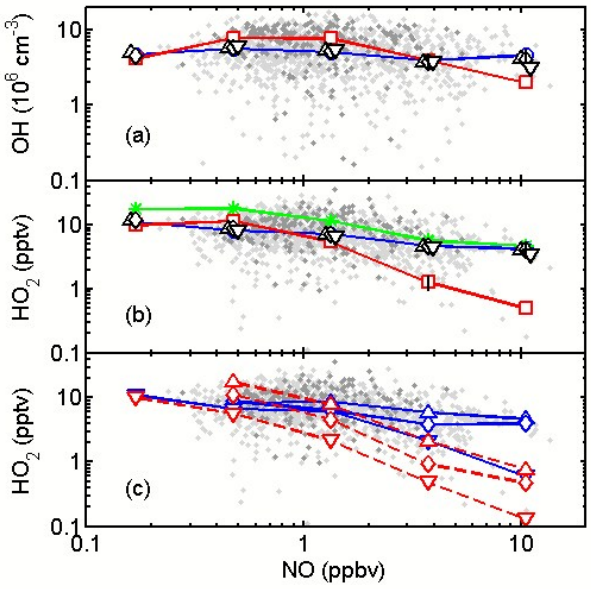

Figure 4. Median behavior of HO_x as a function of NO. (a) OH (10^6 cm^{-3}), measured (blue circles), modeled (red squares), and measured averages of 20-second (upward pointing triangles), 1-minute (diamonds), and 1-hour (downward pointing triangles).; (b) HO_2 (pptv), measured (blue circles), modeled (red squares), measured HO_2 with RO_2 interference (green stars), and measured averages of 20-seconds (upward pointing triangles), 1-minute (diamonds), and 1-hour (downward pointing triangles).; (c) HO_2 (pptv), measured (solid blue lines) and modeled (dashed red lines), for $P(HO_x) > 10^7$ cm^{-3} s^{-1} (upward triangles), 5x10^6 cm^{-3} s^{-1} <$P(HO_x)$ < 10^7 cm^{-3} s^{-1} (diamonds), 1x10^5 cm^{-3} s^{-1} <$P(HO_x)$ < 5x10^6 cm^{-3} s^{-1} (downward triangles). Gray dots are individual 10-min measured data; darker gray dots are data measured between 12:00 and 15:00. Data are filtered for daytime hours between 700 and 17:00.

Measured HO_2 is on average about 7 pptv midday and is within the combined uncertainties of the modeled HO_2. Measured and modeled HO_2 also agree at night, but in the morning, median measured HO_2 is more than twice median modeled HO_2. The HO_2 with RO_2 interference is about twice as large at midday and much larger at night. Thus measured and modeled HO_2 agree within uncertainties for much of the day, if true HO_2 is near the lower bound for measured HO_2.

When median measured and modeled OH and HO_2 are plotted against NO for the daytime, the modeled OH is similar to measured OH for NO up to about 10 ppbv (Figure 4(a)). Measured HO_2 and HO_2*, on the other hand, begin deviating from modeled HO_2 when NO is 1 ppbv and are ~10 times larger when NO is 10 ppbv (Figure 4(b)). This result is consistent with the previous reports of higher-than-expected measured HO_2 for conditions with NO above 1 ppbv. Note that this discrepancy does not depend on uncertainties in

Faraday Discussions Accepted Manuscript

removing the RO_2 interference from the HO_2 signal because HO_2 and HO_2* behave the same way.

HO_2 increases with the increasing production rate of HO_x, $P(HO_x)$, for each value of NO (Figure 4(c)). The 10-minute data are binned into three $P(HO_x)$ ranges: $1x10^5$ cm^{-3} s^{-1} <$P(HO_x)$ < $5x10^6$ cm^{-3} s^{-1}, $5x10^6$ cm^{-3} s^{-1} <$P(HO_x)$ < 10^7 cm^{-3} s^{-1}, and $P(HO_x)$ > 10^7 cm^{-3} s^{-1}. In Bakersfield, these ranges correspond to low $P(HO_x)$ for early morning, late afternoon, or very cloudy days; medium $P(HO_x)$ for mid-morning, midafternoon, or cloudy days; and high $P(HO_x)$ for midday on sunny days. Note that both the measured and modeled HO_2 are greater for greater $P(HO_x)$, as would be expected, but modeled HO_2 is more sensitive to $P(HO_x)$ than measured HO_2 is. Further, in general, the measured-to-modeled HO_2 ratio is least for the highest $P(HO_x)$ and greatest for the lowest $P(HO_x)$. Thus, regions with higher $P(HO_x)$ likely have a measured-to-modeled HO_2 ratio that is closer to 1 even for higher NO values.

These differences between measured and modeled OH and HO_2 are within the widely varying range of previous studies[40]. Even this behavior as a function of $P(HO_x)$ is the same as in previous studies. The CalNex results are quite similar to what is observed in an April 2009 SHARP study in Houston TX.[17] An important difference between Houston and Bakersfield studies is the higher daytime levels of NO in the Bakersfield study, levels that are closer to those observed in New York City in summer 2001.[15] This difference influences the $P(O_3)$ sensitivity to NO_x and VOCs.

Comparison of measured to modeled OH reactivity

The median measured OH reactivity was greatest at night when the atmospheric boundary layer height was lowest and was least during the late afternoon when the boundary layer height was greatest. The median measured OH reactivity was as high at 26 s^{-1} at 4:00, dropped from 15 s^{-1} to 11 s^{-1} between 8:00 and 10:00, then slowly decreased to 9 s^{-1} at 17:00, after which it began a slow increase to nighttime values. Mean values are ~20% higher because of the few large spikes. From day-to-day, OH reactivity varied from 5 s^{-1} to more than 50 s^{-1} at night and from about 3 to 20 s^{-1} during the day. The lowest values were on the few cool rainy days in May. The spikes in OH reactivity generally correlate to NO spikes, suggesting that OH reactivity in Bakersfield is largely due to anthropogenic emissions and combustion,[41] but oxidation products, potentially from biogenic emissions from natural and agricultural sources, have large contributions to reactivity with high ambient temperatures.[25]

This measured OH reactivity is compared to the OH reactivity calculated from the measured chemical species and the modeled products of those measured chemical species. The ratio of model-calculated OH reactivity to measured OH reactivity is 0.59 at night and 0.53 during the day. In a cooler, rainy period at the beginning of the study (before doy 150, 30 May), measured and calculated OH reactivity agreed to within 10%. The missing OH reactivity tends to be greater when the temperature and ozone are higher, but these correlations are weak, suggesting that other factors such as unmeasured species may be contributing to the measured OH reactivity.

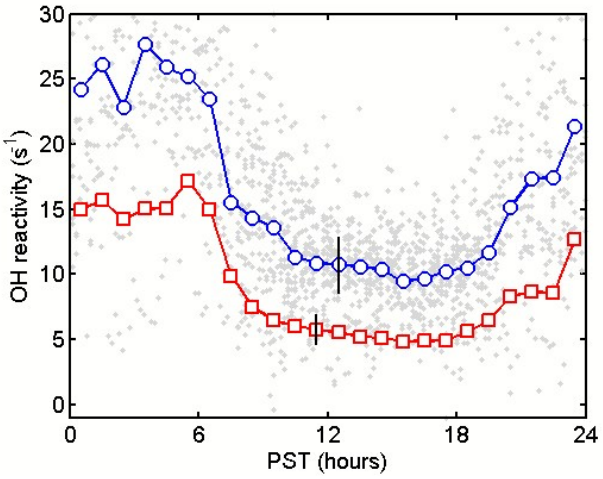

Figure 5. Median diel variation of OH reactivity. Median measured (blue circles) and calculated from modeled chemical species (red squares), with individual 10-min data for measured OH reactivity (gray dots). 339 out of 4392 10-minute data are greater than 30 s^{-1} and are not shown.

If only measured OH reactants are included in the calculated OH reactivity total, the calculated OH reactivity is only slightly less (<10%) than the calculated OH reactivity that includes modeled chemical species. According to the model, 80% of the OH reactivity is caused by 13 chemical species, with the most important being NO_2 (22%), carbon monoxide (11%), formaldehyde (6%), ethanol (8%), methanol (5%), and heptanal+nonanal (5%). The biogenic VOCs isoprene and limonene each contribute less than 2%, thus indicating the dominance of anthropogenic VOCs in the OH reactivity during this study.[25] From this analysis, when NO is high, NO is a major OH sink, accounting for more than half the OH reactivity in some plumes.

The OH reactivity is an indicator of the OH lifetime. For CalNex-SJV, the lifetime was 40 ms during the night and at sunrise and ~100 ms during the day. With winds of 0.5 m s^{-1} during the early morning and 4 m s^{-1} during the rest of the day, OH achieved steady state (>3 lifetimes) for air that had travelled less than 2 meters. However, this view is too simplistic; not only must the lifetime of OH be considered but also the lifetime of OH sources[42] and sudden changes in OH sources and sinks.

The effects on the OH value due to it sources and sinks can be seen by suddenly turning off the photolytic sources of OH and other radicals in a model. Using CalNex-SJV conditions and chemical species, a photochemical box model was run until it achieved steady state and then photolysis was terminated and the run continued for another 100 seconds to follow the decays of OH, HO_2, NO, and other short-lived chemical species

Faraday Discussions Accepted Manuscript

This journal is © The Royal Society of Chemistry 2015

(Figure 6). Initially OH drops at a rate about equal to the OH reactivity until the OH loss rate matches the OH production rate from recycling, primarily HO_2+NO in this case. The OH decay then roughly parallels the decay of its primary source - HO_2 times NO. The half-life of NO is 22 s, HO_2 110 s, and OH 13 s, which is two orders-of-magnitude longer than indicated by the OH reactivity. In this case, the HO_2 half-life is much longer than the NO half-life, but in the morning in CalNex-SJV, the half-life of NO is 60 s, HO_2 13 s, and OH 8 s. Thus, while OH is in steady state with its sources and sinks in less than a second, it abundance is tied to the half-life of its sources as they respond to changes in their sources or sinks.

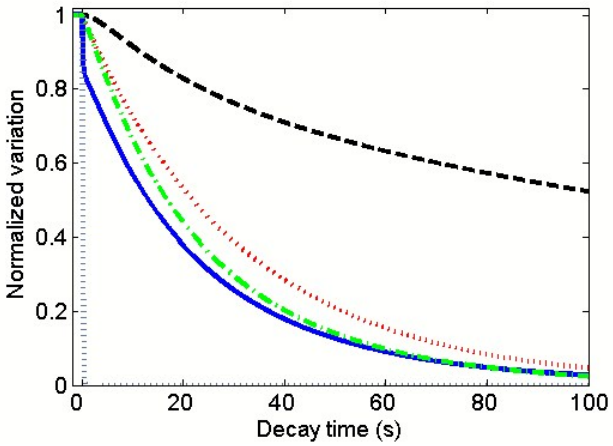

Figure 6. Normalized modeled decays of OH (solid blue), HO_2 (dashed black), NO (dotted red), HO_2 times NO (dot-dashed green), and inverse of OH reactivity (leftmost dotted blue). This case is initialized with O_3 (60 ppbv), NO_2 (2.6 ppbv), NO (1.2 pptv), and OH reactivity (10 s^{-1}).

Typically in model-to-measurement HO_x comparisons, the model is constrained to NO, NO_2, O_3, and all other measured chemical species except OH and HO_2. We have used this method in the analysis for this paper. The model calculates the steady-state values for OH and HO_2. However, HO_2 may not be in steady state because of surface deposition, upwind cloud shadowing, or other HO_x production or loss that occurred within the tens of seconds prior to the measurement. For our example, the typical afternoon wind was 4 m s^{-1}, so that in the HO_2 half-life of 110 s, the HO_2 in an air parcel could be affected during its travel over a distance of almost half a kilometer. Thus HO_2 could have values that are quite different from those calculated by a steady-state model constrained to the measurements made at the field site.

OH production and loss

A critical consistency check of the measurements of OH, HO_2, and OH reactivity is the balance between production and loss for OH. The loss rate for OH is product of the measured OH and OH reactivity; the production rate is all the sum of all the OH sources, including recycling, mostly from HO_2+NO, and primary production, mostly from O_3 photolysis followed by $O(^1D)$+H_2O and HONO photolysis. Most of these quantities and reaction rate coefficients are measured, making this consistency check very close to being independent of the model. The mean measured and modeled OH production and loss rates peaked at (5-9)x10^7 cm^{-3} s^{-1}, (Figure 7(a)). This OH production is lower by a factor of two compared to other US cities and by a factor of 6 compared to Mexico City in 2003.[43] As in previous studies, measured OH production and loss match in the afternoon but not in the morning. From sunrise to almost noon, measured OH production and loss are both two to three times the modeled production/loss and measured OH production is about twice measured OH loss. Because of the short OH lifetime, these two must always match.

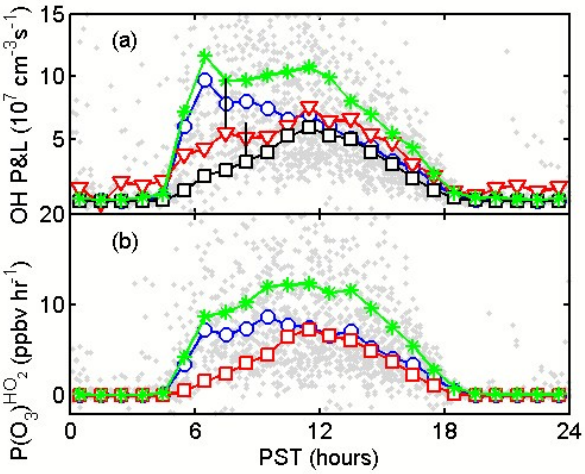

Figure 7. Median diel variation of production and loss. (a) OH (10^7 cm^{-3}), measured OH production (blue circles) and loss (red triangles), measured OH production using HO_2* instead of HO_2 (green stars), modeled production and loss, which are equal (black squares), and individual 10-min production data using measured HO_2 (gray dots); (b) ozone production from HO_2 (pptv), $P(O_3)^{HO2}$ calculated from measured HO_2 (blue circles), modeled HO_2 (red squares), and measured HO_2* (green stars), with individual 10-min data for $P(O_3)^{HO2}$ calculated from measured HO_2 (gray dots).

To resolve this discrepancy, one possibility is that the OH reactivity is biased low when ambient NO is high, which can result from two factors. First, the high OH reactivity in the morning reduces even the initial OH signal by about a decade compared to midday values, so that the low signal-to-noise of the decay and the uncertainty in the subtracted OH background signal strongly influence the calculated OH decays. Laboratory experiments indicate that too little background signal tends to get subtracted when the OH signal is small, causing the calculated decay to be smaller than it should be. Second, the correction factor to account for the recycling of OH by the reaction of HO_2 and ambient NO in the OH reactivity instrument is dependent on NO and the OH reactivity, but it is typically 1.05 to 1.1 for 1 ppbv of NO and increases to 6-10 for 100 ppbv of NO. The uncertainty in the correction factor is estimated to be ±40% (2σ confidence), based on repeated laboratory decays, although we think that this uncertainty can be cut in half. The combination of the tendency for insufficient background subtraction at low OH signals and uncertainty in the NO correction

Faraday Discussions Accepted Manuscript

factor could be responsible for this discrepancy in the balance between OH production and loss. The other possibility is that the HO_2 measurement is in error, which is discussed in a following section.

Ozone production rate

The ozone production from HO_2, $P(O_3)^{HO2}$, is only about half the total $P(O_3)$, the other portion coming from RO_2. We will confine our discussion only to calculated $P(O_3)^{HO2}$ because HO_2 was measured and RO_2 was not. If HO_2 is greater than expected at higher NO values, then by Equation 1.2, $P(O_3)^{HO2}$, should also continue to increase for NO greater than ~1 ppbv, in contrast to the modeled value, which peaks when NO is near 1 ppbv and then decreases. This difference in measured and modeled HO_2 translates directly into a difference in $P(O_3)$ values that are calculated from measured and modeled values of OH and HO_2 (Figure 7(b)). $P(O_3)^{HO2}$ calculated from measured HO_x is lower than $P(O_3)^{HO2}$ calculated from modeled HO_x below ~1 ppbv and then becomes more than a decade larger for NO = 10 ppbv.

Most of this greater-than-expected $P(O_3)^{HO2}$ occurs in the morning before 10:00. The cumulative median $P(O_3)^{HO2}$ shown in Figure 7(b) is 55 ppbv for the model and 97 ppbv for the measurement. This cumulative production can be compared with the mean diel peak O_3 of 58 ppbv (range ±20 ppbv). $P(O_3)$ is about twice $P(O_3)^{HO2}$, so that the cumulative $P(O_3)$ calculated from both modeled and measured HO_2 are more than twice the observed ozone. At any given location, neither the calculated instantaneous nor cumulative ozone production are necessarily related to the peak ozone, which comes from not only the local production but also from production throughout the planetary boundary layer and from transport (Equation 1.1). The calculated $P(O_3)^{HO2}$ suggests that the CalNex_SJV site is in an ozone source region that contributes to the ozone production in the Bakersfield plume as it moves south during the day.

How does this difference in measured and modeled $P(O_3)^{HO2}$ affect the assessment of NO_x-sensitivity or VOC-sensitivity? In four urban areas, both measured and modeled $P(O_3)^{HO2}$ were strongly VOC-sensitive during morning rush hour, but switched to weakly VOC-sensitive or NO_x-sensitive from mid-morning to mid-afternoon.[43] For CalNex-SJV, mean midday NO was typically 1.5 ppbv, so that measured HO_2 was less than twice modeled HO_2. As a result, the greater-than-expected $P(O_3)^{HO2}$ that occurs primarily in the morning does not significantly change the $P(O_3)$ sensitivity to NO_x or VOCs during the 10:00 to 14:00 period used by Pusede et al.[25] in their analysis.

Possible cause of greater-than-expected HO_2 and $P(O_3)^{HO2}$

What could be the cause of the greater-than-expected HO_2 and $P(O_3)^{HO2}$ when NO exceeds 1 ppbv? We look at the five hypotheses presented in the Introduction.

A. HO_2 measurement error

Measured HO_2 could exceed modeled HO_2 if there were an error in the absolute HO_x calibration. However, the HO_2 calibration is tied to the OH calibration and measured OH is approximately equal to the modeled OH. In addition, measured and modeled HO_2 agree within uncertainties in the afternoon, especially if HO_2 is close to the lower limit of possible values. Second, HO_2 is detected by adding internally a few hundred ppmv of NO to convert HO_2 to OH, so the 10 ppbv of atmospheric NO is overwhelmed by the injected NO. Third, a small HO_2 signal offset is not responsible because the general differences between measured and modeled HO_2 in Figure 4 persists even when an offset of 2 pptv is subtracted

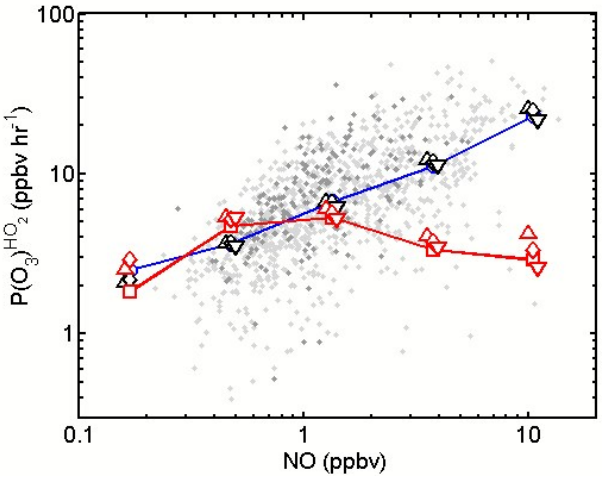

Figure 8. Mean behavior of the ozone production rate due to HO_2, $P(O_3)^{HO2}$, as a function of NO. 10-minute averages of measured (blue circles), modeled (red squares) $P(O_3)^{HO2}$ are plotted along with 20-second (upward pointing triangles), 1-minute (diamonds), and 1-hour (downward pointing triangles) averages. Gray dots are individual 10-min measured data; darker gray dots are data measured between 12:00 and 15:00 when the wind was from the north, although the points with greatest NO generally occurred when the winds were light and out of the east. Data are filtered for daytime hours between 7:00 and 17:00.

from the measured HO_2. Such an offset is not observed and is about a decade higher than the limit-of-detection. Fourth, the RO_2 interference due to alkene and aromatic peroxyl radicals is also unlikely for two reasons. The RO_2 is more rapidly converted to HO_2 as NO increases, but the HO_2 is recycled with OH, so that the RO_2-to-HO_2 ratio decreases as NO increases (Figure 4(b)). Next, a previous study showed these unexpectedly high HO_2 values at higher NO values in the upper troposphere where RO_2 abundances are small.[14] Further evidence is provided by other studies using other instruments and even another HO_2 measurement technique.[9,15,16,18] So far, no HO_2 measurement error has been found that would cause the greater-than-expected decrease in $P(O_3)^{HO2}$ at high NO.

Faraday Discussions Accepted Manuscript

This journal is © The Royal Society of Chemistry 2015

B. Measurement averaging

Does the average of measured HO_2 times the average of measured NO equal the average of HO_2 times NO? This question can be answered by using high-resolution HO_2 and NO measurements and averaging them together. The full width/half maximum (FWHM) of the NO plumes varied from a few seconds to well over an hour. However, for NO plumes with NO greater than 5 ppbv, 80% of time was in plumes that were sampled for more than 20 seconds. As a result, we will use 20 seconds as the minimum time resolution for calculating ns of the products of the averages compared to the averages of the products.

The averages of HO_2 and NO were calculated for 20 seconds, 1 minute, 10 minutes, and 1 hour. These five different averages were plotted as a function of NO for HO_2 in Figure 4 and for calculated $P(O_3)$ in Figure 8. There are no significant differences among the five different averages. Thus, the greater-than-expected HO_2 and $P(O_3)$ at higher NO are not due to averaging over NO plume spikes.

In previous urban studies, point measurements have been compared to long-path absorption measurements to test the assumption that point measurements can adequately represent the integrated chemistry in urban plumes for measurement integration times of minutes or more. In a 1999 study in Nashville TN, long-path and point measurements generally agreed to within 15% or better.[44] In Mexico City in April 2003, point and long-path measurements of several VOCs were in good agreement for time scales of 5 minutes or more, although not for all VOCs.[45,46] While these averages are in space while our averages are in time, the conclusion is that, if there are no unique emission sources nearby, point measurements can represent the photochemistry of an urban region.

C. Conditions when NO_x is not in photostationary state

The theoretical steady-state curve for the HO_2 and $P(O_3)^{HO2}$ versus NO assumes that HO_x production is constant and NO_x is in photostationary state (PSS) as NO changes. Even though NO emissions are typically out of PSS for at most tens of seconds during the day, they are continually coming from thousands of sources and these plumes are continually contributing to ozone production. The analysis presented here makes no assumptions about NO_x PSS. As a result, the measured and modeled curves in Figures 4 and 8 are averages over different HO_x production regimes and may include measurements during conditions when NO_x is not in PSS. However, while NO_x may be out of PSS if we constrain the model-to-measured NO, NO_2, and O_3, the model does calculate steady-state values for HO_2 and OH. So a valid comparison between measured and modeled HO_x requires that HO_x be in steady state but not NO_x.

We tested how close NO_x was to PSS using 1-minute averaged measurements. Comparisons were made between the model with NO, NO_2, and O_3 constrained (i.e., measurements and no assumption of NO_x PSS) to calculations of NO_x PSS. These comparisons show that NO_x was generally within 10-20% of PSS from 8:00 to 14:00, suggesting that NO had decreased about e^{-2}=0.14 from its initial emission. The typical NO lifetime is 20-60 seconds. When these lifetimes are multiplied by the wind speed and by 2, the resulting product is the approximate distance the air must travel from a NO source so that the NO has decreased to 0.14 of its initial value. This distance was in the range of 100-150 m, a distance great enough that several sources could contribute to keep the NO_x slightly out of photostationary state. Because NO_x was not quite in steady state, HO_2 was likely to be in steady state in the morning when its lifetime was 13 s but not in the afternoon when its lifetime was 110 seconds. However, since the greater-than-expected HO_2 occurs primarily in the morning when HO_2 is in steady state, NO_x being out of PSS is not the cause of the greater-than-expected HO_2 and calculated $P(O_3)^{HO2}$.

D Unknown HO_2 sources accompanying NO emissions

Any unknown HO_x sources accompanying NO should show up in the OH reactivity measurement and in the comparison of the balance between OH production and loss (Figure 7(a)). If the accompanying HO_x source is an HO_2 source, such as an aldehyde, then it would also likely be an OH loss and appear in the OH reactivity. However, the agreement between measured and calculated OH reactivity is better when NO is high than when NO is low; calculated OH reactivity accounts for ~50% of measured OH reactivity when NO was less than 1 ppbv but as much as 75% when NO is greater than 10 ppbv, just the opposite of expectations for an unknown HO_2 source that is also an OH loss. Furthermore, an unknown HO_2 source that acts also as an OH loss would cause the measured OH production to exceed the OH loss calculated from the known HO_2 sources, but just the opposite is seen. These arguments are based on OH reactivity measurements that have an uncertain NO correction, so an unknown HO_2 source cannot be entirely ruled out by these observations.

E Missing chemical mechanism

For missing chemistry to cause the greater-than-expected HO_2 dependence on NO, it must have a few characteristics. First, in order for $P(O_3)$ to increase with NO as shown in Figure 8, the HO_2 production must be approximately proportional to NO because the difference between measured and modeled $P(O_3)^{HO2}$ increases about a decade for each decade increase in NO. Second, the HO_2 production rate from this chemistry would need to be approximately $5x10^7$ cm^{-3} s^{-1} in order to balance the HO_2 loss due to the reaction of HO_2 with NO. This value comes from the difference in the OH production with measured and modeled HO_2 (Figure 7(a)). We know of no known chemical mechanism that can satisfy these two constraints. Yet with the uncertainty associated with the products of reactions such as $OH+NO_2$, unknown HO_x-NO_x chemistry is a reasonable possibility for the greater-than-expected HO_2 and calculated $P(O_3)^{HO2}$.

Faraday Discussions Accepted Manuscript

When we first observed this HO_2 discrepancy a decade ago, we hypothesized that it might be due to the reaction sequence

$$OH + NO \rightarrow HONO^* \quad (1.6)$$
$$HONO^* + N_2 \rightarrow HONO \quad (1.7)$$
$$HONO^* + O_2 \rightarrow HO_2 + NO_2 \quad (1.8)$$

The reaction to products HO_2+NO is exothermic, ΔH = -94 kJ mol^{-1}, and, to our knowledge, has never been tested. All studies of OH + NO have been done at either low pressure or in the absence of molecular oxygen, according to Sander et al. and references therein.[46] It is a difficult reaction to study because the HO_2 produced recycles immediately to OH by HO_2 + NO → OH + NO_2. It is difficult to scavenge HO_2 in laboratory studies, so this recycling would appear as a slower rate coefficient for OH+NO+M, although laboratory studies of HONO formation have generally taken known recycling into account.

There is some evidence that this reaction could be occurring. Molecular energy calculations suggest that vibrationally excited HONO ($v_{OH} \geq 3$) can react with O_2 to form HO_2 + NO_2.[48] While this mechanism is a minor HO_2 formation pathway if $HONO^*$ is produced by the photo-excitation of HONO, it could be substantially greater if HONO* is produced by the OH+NO reaction. Other calculations suggest that the H atom can quickly hop from O atom to O atom in sub-nanosecond time scales, about five to ten times faster than the time between collisions with molecular oxygen and that the H atom could transfer to a colliding O_2 molecule.[49] In another study of the OH + acetylene reaction, O_2 reacted with about 25% of the excited-state adducts before they could be collisionally relaxed.[50] These studies suggest that it may indeed be possible for this reaction sequence to occur.

The results of our laboratory studies on this possible reaction have been decidedly mixed. However, the reaction would need to proceed with an effective bimolecular reaction rate of (3-15)x10^{-11} cm^3 $molecule^{-1}$ s^{-1} in order to explain the HO_2/OH ratio observed in this and previous ground-based studies made with GTHOS.

Conclusions

CalNex-SJV provides a good opportunity to compare measured and modeled oxidation chemistry in an environment with plumes of NO_x and their accompanying VOCs and OVOCs. The diel variation of the median measured and modeled OH and HO_2 were generally well represented by the box model constrained by other simultaneous measurements except for HO_2 during morning rush hour. As in many previous studies, the measured HO_2 and the ozone production rate calculated from measured HO_2 decreased much slower than the modeled HO_2 and calculated $P(O_3)^{HO2}$ as a function of NO. The amount of missing OH reactivity was roughly 45% of the total measured OH reactivity. Also as seen in most previous studies, the OH production and loss rates balance in the afternoon and at night, but in the morning, the production greatly exceeds the loss. These discrepancies could arise from issues with transport or issues with chemistry.

The presence of frequent NO_x plumes that lasted from seconds to an hour suggests that transport timescales were comparable to chemical timescales for radicals like NO and HO_2. But even with strong winds (4 m s^{-1}) from a major highway and the urban core NO_x was close to photostationary state as it was sampled at the field site. So, despite the heterogeneity of the sampled air masses, the comparison between the measured and modeled OH and HO_2 was not significantly affected by these plumes in the morning, but may have been affected in the afternoon.

When the OH reactivity is between 5 and 25 s^{-1}, as it was in this study, OH comes into balance with a change in its sources and sinks in much less than a second. However, OH will change only as fast as its sources and sinks change. In this study, the main OH source was HO_2 + NO, so OH had a half-life of 13 seconds because HO_2xNO had a half-life of 16 s. The results from this study show that point measurements can provide a valid test of urban oxidation chemistry if care is taken to ensure that HO_2 is in steady state. NO_x does not have to be in steady-state if NO, NO_2, and O_3 are constrained in the steady state model along with all other simultaneous measurements.

Greater-than-expected HO_2 at high NO results in higher ozone production calculated from measured HO_2, but it does not strongly influence the assessment of midday ozone production sensitivity to NO_x or VOCs. In the morning ozone production is VOC-limited whether modeled or measured HO_2 is used to calculate ozone production. At midday the difference between measured and modeled HO_2 is less, causing at most a small change in the assessment of NO_x-sensitivity or VOC-sensitivity for ozone production.

Unknown HO_x-NO_x chemistry emerged as one of the most likely causes for the greater-than-expected measured HO_2 seen in this and several other previous studies. The proposed reaction of OH+NO+O_2→HO_2+NO_2 could resolve the HO_2 discrepancy; laboratory and modeling kinetic studies are needed to test this hypothesis. This conclusion re-emphasizes the need to re-investigate HO_x-NO_x photochemistry under atmospheric conditions.

Acknowledgements

We thank John Karlik, Rick Ramirez and the other scientists and staff at the University of California Kern County Extension Center for their hospitality and use of their facilities. Participation by WHB, BCB, JT was supported by grants from California Air Resources Board through the University of California, Berkeley (UCB subcontract 00007016) and from NSF (ATM-0706821).

Faraday Discussions Accepted Manuscript

 This journal is © The Royal Society of Chemistry 2015

Please do not adjust margins

Notes and references

1 M.L. Bell, A. McDermott, S.L. Zeger, J.M. Samet, F. Dominici, *J. Am. Med. Assoc.,* 2004, **19**,2372.

2 US EPA *2013 Final Report*, http://cfpub.epa.gov/ncea/isa/recordisplay.cfm?deid=247492#Download, (accessed October 2015).

3 US EPA Air Trends, 2015a www3.epa.gov/airtrends/ozone.html, (accessed November 2015).

4 A.J. Haagen-Smit and M.M. Fox, 1954, J. *Air & Waste Management Association*, **4:3**, 105-136.

5 National Research Council, 1991, *Rethinking the Ozone Problem in Urban and Regional Air Pollution*, Washington, D.C.: National Academy Press.

6 J. Calvert, J. Orlando, W. Stockwell, T. Wallington, 2015, *The Mechanisms of Reactions Influencing Atmospheric Ozone*, Oxford University Press, New York, NY. ISBN: 9780190233020.

7 L. Kleinman, P. Daum, Y. Lee, L. Nunnermacker, S. Springston, J. Weinstein-Lloyd, J. Rudolph, *J. Geo. Res.,* 2001, **107**, 4733.

8 J. Thornton, P. Woolridge, R. Cohen, M. Martinez, H. Harder, W. Brune, E. Williams, J. Roberts, F. Fehsenfeld, S. Hall, R. Shetter, B. Wert, A. Fried, 2002, *J. Geo. Res.*, **107**, 4146.

9 M. Martinez, H. Harder, T. Kovacs, J. Simpas, J. Bassis, R. Lesher, W. Brune, G. Frost, E. Williams, C. Stroud, B. Jobson, J. Roberts, S. Hall, R. Shetter, B. Wert, A. Fried, B. Alicke, J. Stutz, V. Young, A. White, R. Zamora, 2003, *J. Geo. Res., **108**, 4617.*

10 I. Pollack, T. Ryerson, M. Trainer, D. Parrish, A. Andrews, E. Atlas, D. Blake, S. Brown, R. Commane, B. Daube and Coauthors, 2012, *J. Geo. Res.* **, 117**, D00V05.

11 D. Tong and D. Mauzerall, 2006, *Atmos. Environ.***, 40**, 3041.

12 K. Appel, A.B. Gilliland, G. Sarwar, R.C. Gilliam, *Atmos Environ.*,2007, **41**, 9603.

13 U. Im, R. Bianconi, E. Solazzo, I. Kioutsioukis, A. Badia, A. Balzarini, R. Baro, R. Bellasio, D. Brunner, C. Chemel and Coauthors, 2015, *Atmos. Environ.*, **115**, 404.

14 I. Faloona, D. Tan, W. Brune, L. Jaegle, D. Jacob, Y. Kondo, M, Koike, R. Chatfield, R. Pueschel, G. Ferry, G. Sachse, S. Vay, B. Anderson, J. Hannon, H. Fuelberg, 2000, *J. Geo. Res. **, 105,** 3771.*

15 X. Ren, H. Harder, M. Martinez, R. Lesher, A. Oliger, J. Simpas, W. Brune, J. Schwab, K. Demerjian, Y. He, X. Zhou, H. Gao, 2003, *Atmos. Env.,* **37**, 1352.

16 K.M Emmerson, N. Carslaw, L.J. Carpenter, D.E. Heard, J.D. Lee, M.J. Pilling, 2005, *J. Atm. Chem.*, **52**, 143-164.

17 X. Ren, D. van Duin, M. Cazorla, S. Chen, J. Mao, L. Zhang, W. Brune, J. Flynn, N. Grossberg, B. Lefer, B. Rappenglück, K. Wong, C. Tsai, J. Stutz, J. Dibb, B. Thomas Jobson, W. Luke, P. Kelley, 2013, *J. Geo. Res.,* **118**, 5770.

18 Y. Kanaya, R. Cao, H. Akimoto, M. Fukuda, Y. Komazaki, Y. Yokouchi, M. Koike, H. Tanimoto, N. Takegawa, Y. Kondo, 2007, *J. Geo. Res.*, **112**, D21312, doi:10.1029/2007JD008670.

19 K. M. Spencer, D. C. McCabe, J. D. Crounse, J. R. Olson, J. H. Crawford, A. J. Weinheimer, D. J. Knapp, D. D. Montzka, C. A. Cantrell, R. S. Hornbrook, R. L. Mauldin III, P. O. Wennberg, 2009, *Atmos. Chem. Phys.*, **9**, 3697–3707

20 M. Cazorla, W.H. Brune, 2010, *Atmos. Meas. Tech.*, **3**, 545-555.

21 M. Cazorla, W. Brune, X. Ren, B. Lefer, 2012, *Atmos. Chem. Phys.,* **12**, 1203.

22 D.R. Gentner, G. Isaacman, D.R. Worton, A.W.H. Chan, T.R. Dallmann, L. Davis, S. Liu, D.A. Day, L.M. Russell, K.R. Wilson, R. Weber, A. Guha, R.A. Harley, A.H. Goldstein, 2012, *Proceedings of the National Academy*, **109,** 18318-18323.

23 US EPA, 2015b, *AirData, http://www3.epa.gov/airquality/airdata/ (accessed November 2015).*

24 S. E. Pusede, R.C. Cohen, 2012, *Atmos. Chem. Phys*., **12**, 8323-8339.

25 S. E. Pusede, D.R Gentner, P.J. Woolridge, E.C. Browne, A.W. Rollins, K.-E. Min, A.R. Russell, J. Thomas, L. Zhang, W.H. Brune, and Coauthors, 2014, *Atmos. Chem. Phys.*, **14**, 3373-3395.

26 I. Faloona, D. Tan, R. Lesher, N. Hazen, C. Frame, J. Simpas, H. Harder, M. Martinez, P. Di Carlo, X. Ren, W. Brune, 2004, *J. Atmos. Chem.,* **47**, 139.

27 H. Fuchs, B. Bohn, A. Hofzumahaus, F. Holland, K. Lu, S. Nehr, F. Roher, A Wahner, 2011, *Atmos. Meas. Tech.*, **4**, 1209.

28 S.M. Griffith, R.F. Hansen, S. Dusanter, P.S. Stevens, M. Alaghmand, S.B. Bertman, M.A. Carroll, M. Erickson, M. Galloway, N. Grossberg, and Coauthors, 2013, *Atmos. Chem. Phys.*, **13**, 5403-5423, doi:10.5194/acp-13-5403-2013.

29 T. Kovacs and W. Brune, 2001. *J. Atmos. Chem.*, **39**, 105.

30 Mao J., X. Ren, W.H. Brune, J. R. Olson, J. H. Crawford, A. Fried, L. G. Huey, R. C. Cohen, B. Heikes, H. B. Singh, D. R. Blake, G. W. Sachse, G. S. Diskin, S. R. Hall, and R. E. Shetter, 2009, *Atmos. Chem. Phys.*, **9**, 163-173.

31 T. Shirley, W. H. Brune, X. Ren, J. Mao, R. Lesher, B. Cardenas, R. Volkamer, L. T. Molina, M. J. Molina, B. Lamb, E. Velasco, T. Jobson, and M. Alexander, 2006, *Atmos. Chem. Phys.*, **6**, 2753-2765.

32 T. Ryerson, A. Andrews, W. Angevine, T. Bates, C. Brock, B. Cairns, R. Cohen, O. Cooper, J. de Gouw, F. Fehsenfeld, 2013, *J. Geo. Res.,***118**, 5830.

33 M. Jenkin, S. Saunders, M. Pilling, 1997, *Atmos. Env.,* **31**, 81.

34 G.M Wolfe, J.A. Thornton, 2011, *Atmos. Chem. Phys.*, **11**, 77–101.

35 J. Mao, X. Ren, L. Zhang, D. M. Van Duin, R. C. Cohen, J.-H. Park, A. H. Goldstein, F. Paulot, M. R. Beaver, J. D. Crounse, and Coauthors, 2012, *Atmos. Chem. Phys.*, **12**, 8009–8020.

36 S. Madronich, S. Flocke, 1999, *Environmental Photochemistry*, Springer Berlin Heidelberg.

37 R.E. Shetter, L. Cinquini, S.R. Hall, S. Madronich, 2002, *J. Geophys. Res.*, **107**, PEM 6-1-PEM 6-12, DOI: 10.1029/2001JD001320.

38 S. Chen and W.H. Brune, 2012, *Atmos. Env.*, **55**, 288-296, DOI: 10.1016/j.atmosenv.2012.03.061.

39 K. Hens, A. Novelli, M. Martinez, J. Auld, J. R. Axinte, R. Bohn, B. H. Fischer, P. Keronen, D. Kubistin, A.C Nölscher, and Coauthors, 2014, *Atmos. Chem. Phys.*, **14**, 8723–8747, doi:10.5194/acp-14-8723-2014.

Faraday Discussions Accepted Manuscript

Please do not adjust margins

40 Stone, D., L.K. Whalley, D.E. Heard, 2012, *Chem. Soc. Rev.*, **41**, 6348-6404.
41 D.R. Gentner, T.B. Ford, A. Guha, J. Brioude, W.M. Angevine, J.A. de Gouw, C. Warneke, J.B. Gilman, T.B. Ryerson, J. Peischl, S. Meinardi, D.R. Blake, E. Atlas, W.A. Lonneman, T.E. Kleindienst, M.R. Beaver, J.M. St. Clair, P.O. Wennberg, T.C. VandenBoer, M.Z. Markovic, J.G. Murphy, R.A. Harley, A.H. Goldstein, 2014, *Atmos. Chem. Phys.*, **14**, 4955-4978, doi:10.5194/acp-14-4955-2014.
42 N. Bell, D.E. Heard, M.J. Pilling, and A.S. Tomlin, 2003, *Atmospheric Environment*, **37**, 2193-2205.
43 J. Mao, X. Ren, S. Chen, W.H. Brune, Z. Chen, M. Martinez, H. Harder, B. Lefer, B. Rappengluck, J. Flynn, M. Leuchner, 2010, *Atmospheric Environment*, **44**, 4107.
44 J.A. Thornton, J. A., P. J. Wooldridge, R. C. Cohen, E. J. Williams, D. Hereid, F. C. Fehsenfeld, J. Stutz, and B. Alicke, 2003, *J. Geo. Res.*, **108**, 4496, doi:10.1029/2003JD003559.
45 E. Velasco, B. Lamb, H. Westberg, E. Allwine, G. Sosa, J. L. Arriaga-Colina, B. T. Jobson, M. L. Alexander, P. Prazeller, W. B. Knighton, T. M. Rogers, M. Grutter, S. C. Herndon, C. E. Kolb, M. Zavala, B. de Foy, R. Volkamer, L. T. Molina, and M. J. Molina, 2007, *Atmos. Chem. Phys.*, **7**, 329-353.
46 B. T. Jobson, R. A. Volkamer, E. Velasco, G. Allwine, H. Westberg, B. K. Lamb, M. L. Alexander, C. M. Berkowitz, and L. T. Molina, 2010, *Atmos. Chem. Phys.*, **10**, 1989-2005.
47 S.P. Sander, S. P., J. Abbatt, J. R. Barker, J. B. Burkholder, R. R. Friedl, D. M. Golden, R. E. Huie, C. E. Kolb, M. J. Kurylo, G. K. Moortgat, V. L. Orkin and P. H. Wine, 2012, JPL Publication 10-6, Pasadena, CA, http://jpldataeval.jpl.nasa.gov.
48 M. Staikova, D.J. Donaldson, J.S. Francisco, 2002, *J. Phys. Chem. A*, **106**, 3023-3028.
49 Y. Miller, G. M. Chaban, B. J. Finlayson-Pitts,|and R. B. Gerber, 2006, *J. Phys. Chem. A*, **110**, 5342-5354.
50 D.R. Glowacki, J. Lockhart, M. A. Blitz, S.J. Klippenstein, M.J. Pilling, S.H. Robertson, P.W. Seakins, 2012, *Science,* **337**, 1066, DOI: 10.1126/science.1224106.

Faraday Discussions Accepted Manuscript

This journal is © The Royal Society of Chemistry 2015